## REMARKS

Applicants have amended claim 1 to more particular point out and distinctly claim the subject matter. Support for the amendment can be found at page 8, lines 1-7 and page 16, lines 22-28 of the original Specification. This amendment has necessitated the cancellation of claims 4, 8-9, and 17-18. Applicants have also corrected minor deficiencies in claims 1, 2, 10, 12, and 13. No new matter has been introduced by the amendments.

The phrase "mixing 55 to 80 wt part alphamethyl styrene, ... in a polymerization reactor," a limitation of amended claim 1, is essentially the same as that recited in original claim 17. The phrase "wherein the copolymer comprises ... chain," another limitation of amended claim 1, is essentially the same as that recited in original claim 4. **Thus, the proposed amendments should be entered as they raise no new issues that will require further consideration or search and also do not touch the merits of the application within the meaning of 37 C.F.R. § 1.116(b).**

Claims 1-3, 5-7, and 10-16 are currently pending. Reconsideration of the application, as amended, is respectfully requested in view of the remarks below.

Rejection under 35 U.S.C. § 112, second paragraph

Claims 1-18 are rejected under 35 U.S.C. § 112, second paragraph as being indefinite. Specifically, the Examiner points out that "[t]he term 'heat resistant' is relative and subjective and therefore unclear." See the Office Action, page 2, line 21 to page 3, line 2.

Applicants have removed this term from claims 1 (three occurrences) and 10 (one occurrence). It is submitted that claims 1-3, 5-7, and 10-16 are no longer indefinite and that this rejection should be withdrawn.

Rejection under 35 U.S.C. § 112, first paragraph

Claims 1-18 are rejected under 35 U.S.C. § 112, first paragraph on four grounds. See the Office Action, page 2, lines 2-20. Applicants respectfully traverse each ground below:

(1) The Examiner points out that "[t]he level of 15% of aromatic vinyl aromatic vinyl aromatic vinyl chain structure is not disclosed by the specification as filed but rather the

specification as filed only refers to a level of alphamethylstyrene units." Applicants have replaced the phrase "less than 15% of aromatic vinyl-aromatic vinyl-aromatic vinyl chain structure" with "less than 15% of alphamethyl styrene-alphamethyl styrene-alphamethyl styrene chain" in claim 1.

(2) According to the Examiner, "Applicants' level of 45% or less of aromatic vinyl ... vinyl cyanide vinyl cyanide chain structure is not disclosed by the specification as filed but rather only levels of alphamethylstyrene instead of aromatic vinyl is disclosed ...." Applicants have canceled claim 18, which contains the phrase "45% or less of aromatic vinyl-vinyl cyanide-vinyl cyanide chain", and included in claim 1 the phrase "45% or less of alphamethyl styrene-acrylonitrile-acrylonitrile chain."

(3) The Examiner asserts that "[t]he limitation that applicants' particle sizes are number average particle sizes is not disclosed by the specification as filed as recited in at least claim 2." Applicants disagree. According to the original Specification, the particle sizes of the rubber latex were measured using Nicomp (Model: 370HPL) by a dynamic laser-light scattering method. See page 10, lines 25-27. Indeed, particle sizes obtained using Nicomp (Model 370) by a dynamic light scattering method are number average particle sizes. See, e.g., Kirsch et al., *Acta Polym.* 1999, 50, 347 (at 348, the third last paragraph in the left column), a copy of which is attached hereto as "Exhibit A." In other words, one skilled in the art would know that the particle sizes disclosed in the original Specification are number average particle sizes.

(4) According to the Examiner, "[t]he particle size of 600 Angstroms as recited in at least claim 12 is not disclosed by the specification as filed." Applicants disagree. Contrary to the Examiner's assertion, the number 600 Å appears at page 5, line 24 of the original Specification.

For the reasons and facts set forth above, Applicants request withdrawal of this rejection.

Rejection under 35 U.S.C. § 102(b) and 35 U.S.C. § 103(a)

The Examiner rejects claims 1-18, relying on two references independently. In response, Applicants have amended claim 1, the broadest claim, to narrow its scope. More specifically, Applicants have limited claim 1 to specific reaction conditions, i.e., specific starting materials and their amounts, specific temperatures, and specific reaction times. Under these conditions, only a specific copolymer is obtained. Indeed, Applicants have narrowed the copolymer thus

obtained from an aromatic vinyl-vinyl cyanide copolymer to an alphamethyl styrene-acrylonitrile copolymer. This copolymer is further narrowed to less than 15% alphamethyl styrene-alphamethyl styrene-alphamethyl styrene chain and 45% or less alphamethyl styrene-acrylonitrile-acrylonitrile chain.

In view of the just-mentioned amendments, Applicants submit that claim 1, as well as its dependent claims, is patentable over the two references cited by the Examiner. Applicants respectfully traverse each reference below.

**I**

Claims 1-18 are rejected as being anticipated by, or as being obvious over Padwa et al., U.S. Patent 5,910,538 ("Padwa"). See the Office Action, page 3, lines 23-25.

Amended claim 1, the only independent claim, will be discussed first. It is drawn to a method for preparing a thermoplastic resin composition. The method includes (a) preparing a graft ABS polymer by emulsion polymerization of (i) 40 to 70 wt parts conjugated diene rubber latex, (ii) 15 to 40 wt parts an aromatic vinyl compound, and (iii) 5 to 20 wt parts a vinyl cyanide; (b) preparing a copolymer by: (i) mixing 55 to 80 wt part alphamethyl styrene, 20 to 45 wt part acrylonitrile, 26 to 30 wt parts a solvent, and 0.1 to 0.5 wt parts a molecular weight controlling agent in a polymerization reactor, and (ii) conducting a mass polymerization at 140~170°C for 2~4 hours; in which the copolymer contains less than 15% alphamethyl styrene-alphamethyl styrene-alphamethyl styrene (AMS-AMS-AMS) chain and 45% or less alphamethyl styrene-acrylonitrile-acrylonitrile (AMS-AN-AN) chain; and (c) blending the graft ABS polymer and the copolymer.

The Examiner concedes that Padwa does not explicitly disclose "applicants' level of vinyl aromatic vinyl aromatic vinyl aromatic chain structure [in the compatibilizer]." See the Office Action, page 6, lines 23-24. However, the Examiner points out that "patentees' processes inherently produce materials having applicant's level of vinyl aromatic vinyl aromatic vinyl aromatic chain structure." See the Office Action, page 7, lines 6-8. Applicants disagree.

Padwa discloses that a compatibilizer (a terpolymer) can be prepared by polymerizing styrene , acrylonitrile, and maleic anhydride (a third monomer) in the presence of methylethyl ketone (a solvent) and isooctyl thioglycolate (a chain transfer agent) at 145°C. See column 8, lines 30-35. However, the method described in Padwa would not necessarily produce a

copolymer containing less than 15% AMS-AMS-AMS chain and 45% or less AMS-AN-AN chain, which is required by amended claim 1. More specifically, it is well known in the art that AMS has a depolymerization temperature (61°C) much lower than that of styrene (310°C). See Table 3-13 at page 254 of Odian, "Principles of Polymerization" 1970. A copy of this page is attached hereto as "Exhibit B." Thus, when preparing an AMS-AN copolymer at high temperature, AMS-AMS-AMS chain in the copolymer tends to depolymerize, leading to the formation of higher amount of AMS-AN-AN chain. As a result, replacing styrene with AMS would not necessarily produce a copolymer containing less than 15% AMS-AMS-AMS chain and 45% or less AMS-AN-AN chain under the conditions described in Padwa. By contrast, the method of amended claim 1 uses a unique composition to produce a copolymer containing less than 15% AMS-AMS-AMS chain and 45% or less AMS-AN-AN chain. A copolymer containing such unique structural characteristics has superior thermal stability. See page 8, line 23 to page 9, line 4 of the original specification. In other words, these structural characteristics are not inherent in the compatibilizer disclosed in Padwa. Thus, Padwa does not disclose or suggest a copolymer having the unique structural characteristics required by amended claim 1.

For the reasons set forth above, claim 1 is not anticipated or rendered obvious by Padwa. As claims 2-3, 5-7, and 10-16 depend from claim 1, they are also not anticipated or rendered obvious by Padwa.

**II**

Claims 1-11 and 18 are rejected as being anticipated by, or as being obvious over Leitz et al., U.S. Patent 5,605,963 ("Leitz"). See the Office Action, page 4, lines 21-23.

As mentioned above, amended claim 1 is drawn to a method for preparing a thermoplastic resin composition, which includes a copolymer containing less than 15% AMS-AMS-AMS chain and 45% or less AMS-AN-AN chain.

Leitz discloses an ABS polymer composition having polymers A, B, C, and D. The Examiner pointed out that "patentees' component C is preferably produced by solution polymerization or mass polymerization at column 2 lines 55-67. Given the similarities of applicants' and patentees' process, it would reasonably appear that applicants' and patentees' characteristics are inherently the same." See the Office Action, page 5, lines 9-15. Applicants disagree.

Leitz does not disclose or suggest, in the above-mentioned passage, a process that can prepare a copolymer containing less than 15% AMS-AMS-AMS chain and 45% or less AMS-AN-AN chain, which is required by amended claim 1. Indeed, Leitz discloses in the actual Example that component C is prepared by polymerizing styrene and acrylonitrile without giving any specific reaction conditions. As discussed above, AMS has a depolymerization temperature (61°C) much lower than that of styrene (310°C). Therefore, replacing styrene with AMS would not necessarily result in a copolymer containing less than 15% AMS-AMS-AMS chain and 45% or less AMS-AN-AN chain. Thus, in view of the teachings of Leitz, one skilled in the art would not have come up with the unique compositions recited in amended claim 1 to produce a copolymer having these unique structural characteristics.

Thus, claim 1 is not anticipated or rendered obvious by Leitz. Neither are claims 2-3, 5-7, and 10-16 dependent from it.

## CONCLUSION

Applicants submit that the grounds for rejection asserted by the Examiner have been overcome, and that claims 1-3, 5-7, and 10-16, as pending, define subject matter that is definite, enabled, novel, and non-obvious. On this basis, it is submitted that all claims are now in condition for allowance, an action of which is requested.

Please apply any other charges to deposit account 06-1050, referencing Attorney's Docket No. 12652-006US1.

Respectfully submitted,

Date: 2-10-04

Y. Rocky Tsao

Y. Rocky Tsao, Ph.D., J.D.
Attorney for Applicants
Reg. No. 34,053

Fish & Richardson P.C.
225 Franklin Street
Boston, MA 02110-2804
Telephone: (617) 542-5070
Facsimile: (617) 542-8906
20782776.doc

# Full Papers

## Particle morphology of carboxylated poly-(*n*-butyl acrylate)/poly(methyl methacrylate) composite latex particles investigated by TEM and NMR

*S. Kirsch*[+], *K. Landfester*[++], *O. Shaffer* and *M.S. El-Aasser*

Emulsion Polymers Institute and Department of Chemical Engineering, Lehigh University, Bethlehem, Pennsylvania 18015, USA
[+] Present address: BASF Aktiengesellschaft, ZKD-Forschung, Dispersionen, D-67056 Ludwigshafen, FRG
[++] Present address: Max Planck Institute of Colloids and Interfaces, D-14424 Golm, FRG

Particles with a copolymer soft core of poly(*n*-butyl acrylate)/poly(methyl methacrylate) (PBA/PMMA) and a homopolymer hard shell of PMMA were characterized using transmission electron microscopy and solid-state NMR spectroscopy. Two synthesis parameters were investigated: (1) the phase ratio of the core and the shell and (2) the compatibility of the two phases. A series of core-to-shell ratios from 100/0 to 25/75 were synthesized and characterized. The compatibility between the phases was changed (1) by using acrylic acid in either the core and the shell or in both, (2) by synthesizing a homopolymer or a copolymer core or (3) by introducing crosslinking points in the core. The combination of transmission electron microscopy and solid-state NMR spectroscopy allows quantitative determination of the extent of coverage of the core by the shell polymer and the interphase thickness; both were found to depend on the shell content and the compatibility of the phases.

### 1. Introduction

Composite latex particles are widely used in industrial applications, e.g., paints, coatings, and adhesives, in order to achieve latex film properties which can not be achieved by a physical blend of two or more different polymer components. The most common process to synthesize composite latex particles is seeded emulsion polymerization. This technique allows one to create particles in a well defined way regarding the resulting particle size. By using different monomer compositions at different stages in a seeded emulsion polymerization, gives one the ability to achieve complex particle morphologies (phase distributions within a particle). In most cases, the resulting particle morphology can not be described simply as a core/shell type. This is due to an interplay of thermodynamic as well as kinetic parameters during the polymerization process [1]. Transition morphologies, i.e., morphologies in-between the limits of complete phase separation and core/shell type particles, such as hemispherical, raspberry, mushroom- and confetti-like particles are described in the literature [2]. One major theoretical approach for predicting the resulting particle morphology is to take advantage of the contributions of the interfacial and surface free energies which determine the thermodynamic driving forces for morphology development. Many efforts have been made to calculate these free energy contributions and to predict the final phase distributions in a particle [3, 4]. One experimental approach to increase the phase compatibility is the use of grafted macromonomers (PBA backbone with PMMA macromonomer side chains) during a miniemulsion polymerization process [5, 6]. In the current work, a conventional emulsion polymerization process was used and the phase compatibility was increased by using a PBA/PMMA (66:34) copolymer seed in a second stage polymerization. Due to the chemical similarity between the two phases, this approach makes it difficult to determine the particle morphology. Thus, a combination of characterization techniques of transmission electron microscopy (TEM) with various staining methods and solid state NMR, were used to examine the particle morphologies in the current latex system.

Because of their small size, colloidal particles synthesized by an emulsion polymerization process are readily observed using transmission electron microscopy (TEM) which allows observation of the particle morphology. The advantages of TEM are the following: (i) high resolution which allows one to determine the particle size and particle size distribution as well as to obtain detailed information about the particle surface properties; and (ii) in contrast to scattering methods, the observation of the particles in real space which leads to more direct information. TEM results depend strongly on the ability to induce a contrast between different structures, through different electron densities in the particle. This is usually accomplished by using different staining techniques which rely on different chemical reactivities of the different polymer phases with the staining agent [1, 7]. However, for our samples, there are only slight differences in the reactivity of the staining agents to the different phases. The platinum (Pt) shadowing technique in contrast, determines only the particle shape at the time of the staining which can sometimes be related to the particle morphology. Therefore, different staining techniques were used to obtain different kinds of information [1].

Solid-state NMR methods based on $^1H$ spin-diffusion experiments have been developed for the characterization of heterogeneities in polymers and polymer blends [8]. They also have been used for polymer particles produced by two-step emulsion polymerization [9]. The dipolar filter used for the spin-diffusion experiment is sensitive to different polymer chain mobilities in the system caused by differences in the glass transition temperatures, $T_g$, of different types of polymers. By varying the filter strength in the spin-diffusion experiment one is able to obtain detailed information about the particle morphology [10, 11]. Due to the very high spatial resolution of the method, it is also possible to resolve interfacial as well as domain structures on the nanometer scale-level within the particles. In this

  0323-7648/99/1010-0347$17.50+.50/0 

paper the NMR spin diffusion results were combined with the TEM measurements in order to determine the extent of surface coverages of the seed particles with the shell polymer in a composite latex system synthesized in multiple step emulsion polymerization processes.

## 2. Experimental

### 2.1. Chemicals

All synthesis were performed in a 250 ml four-necked flask equipped with a reflux condenser, $N_2$-gas inlet tube, PTFE stirrer at 120 rpm, adjustable inlet funnel to feed the pre-emulsions and a feeding tube for the initiator solution. The initiator was fed at a constant feeding rate of 0.05 ml/min by a syringe Harvard Apparatus 22 feeder.

Methylmethacrylate (MMA), *n*-butylacrylate (BA) monomers (Aldrich) were purified by passing through a column filled with an inhibitor-remover packing (Aldrich). Acrylic acid (AA, Aldrich), sodium dodecyl sulfate (SDS, Fischer Chemical), sodium persulfate (NaPS, FMC Corporation), sodium pyrophosphate (NaPP, Aldrich) and concentrated aqueous solution of ammonia (20%, Fischer Chemical) are used as received without further purification. All pre-emulsions are homogenized by ultrasonification (sonifier from Bransons Sonic Power & Co, output level 7) and no creaming of the unstirred pre-emulsion could be observed until the end of the feeding process.

### 2.2. Equipment

The particle size and particle size distribution were measured via dynamic light scattering (DLS) and capillary hydrodynamic fractionation (CHDF). For DLS measurements a Nicomp submicron particle sizer (Model 370) was used. All samples for CHDF (1100, Matec Applied Science) were prepared by diluting the original emulsion to 5% solid, sonicated in a sonifier bath (Commonwealth Scientific) to break up clusters of colloidal particles and were passed through a 5 μm filter (Millipore). All particle sizes obtained by DLS and CHDF are reported as number average diameter.

For the TEM experiments a Philips EM 400 at an acceleration voltage of 100 keV was used. All images were taken at a magnification of 60000 or 120000. Some latex samples were cleaned by using a filtration unit (Advantec MFS Inc., type UHP-76) to remove all water soluble oligomers from the emulsion. All latex samples were diluted to 3% solids and washed with deionized (DI) water in a filtration cell using a polycarbonate Nuclepore membrane with a pore size of 0.1 μm.

$^1$H and $^{13}$C NMR solid-state spectra were recorded on a General Electric GN-300 NMR spectrometer equipped with a standard Doty MAS probe head. All samples were spun at a frequency of 3 kHz. The 90° pulse lengths were in the range of 3.5 to 4.0 μs. Dipolar broadband decoupling (DD) was used to eliminate $^1$H-$^{13}$C dipolar coupling. The spin-diffusion experiments were carried out with selection of the mobile poly(butyl acrylate) (PBA) using the dipolar filter which consists of a pulse sequence with 12 90° pulses separated by a delay time, $t_d$, varying between 2 and 80 μs. Typically, 100–200 scans for the $^1$H spectra were accumulated with a repetition time of 2 s.

### 2.3. Synthesis and characterization of the composite latex particles

The PBA/PMMA composite latex particles were prepared by a conventional semi-batch emulsion polymerization process. The recipe for the standard 75/25 soft-to-hard phase ratio particles is described below. The recipes for the variations can be calculated from the data given in Table 1.

For the soft (PBA/PMMA) seed particles, 2 g of the first stage material (see below), 27 g water, 0.5 g of a 15 wt.% of aqueous solution of SDS and 1 g of the initiator solution (0.545 mM aqueous solution of NaPS) were mixed together and allowed to react at 85 °C for 15 min.

The first stage pre-emulsion was prepared from 15.2 g water, 6.3 g SDS solution, 5.1 mM acrylic acid, 0.125 mol MMA and 0.2 mol *n*BA. The first stage was buffered by adding 3.3 g of a 0.2 wt.% solution of NaPP. The pre-emulsion and 3.73 g initiator solution were fed to the reaction mixture over a period of 2 h.

The second stage pre-emulsion consists of 5.8 g water, 0.7 g SDS solution, 5.1 mM acrylic acid and 0.125 mol MMA. Following the end of the addition of the first stage pre-emulsion, the second stage mixture was fed along with 1.4 g initiator solution into the reaction vessel over a period of 45 min.

After the polymerization, the latexes were neutralized to pH 7 and then allowed to cool down to room temperature (RT).

The results of the DLS as well as the CHDF measurements for the final latex particles, $D_n$, with different soft-to-hard phase ratios are given in Table 1. A good agreement between most of the DLS and CHDF measurements is evident. No systematic dependence of the particle size on the soft-to-hard phase ratio can be detected. The CHDF measurements always gave a Gaussian particle size distribution with a standard deviation ranging from $\sigma = 0.1$ to 0.2.

### 2.4. Sample preparation

#### *2.4.1. TEM-experiments*

Different staining techniques were used to enhance the contrast of certain phase regions in the colloidal particles:

For the *negative staining*, the particles were treated with a 2 wt.% (percent by weight) aqueous solution of uranyl acetate (UAc) (Fluka). For sample preparation, the original latex was highly diluted until a hardly visible turbidity was reached. One drop of the diluted and strained sample was placed onto the copper (Cu) grid. The wet samples were then placed directly into the TEM-sample holder equipped with a cold stage unit. This cold stage unit, cooled by liquid

Table 1. Chemical composition of the first and the second stage polymerization and final particle size. The total DI water used for the pre-emulsions was 21 g, the amount of DI water in both stages can be calculated from the given soft to hard phase ratio. The overall amount of the 15 wt.% aqueous SLS solution was 7 g.

| Sample soft/hard wt.% | SLS [g] | AA [mmole] | MMA [mole] | BA [mole] | SLS [g] | AA [mmole] | MMA [mole] | DLS $d$ [nm] | CHDF $d$ [nm] | $T_g$ [°C] |
|---|---|---|---|---|---|---|---|---|---|---|
| | first stage | | | | second stage | | | | | |
| 100/0 | 7 | 10.3 | 0.166 | 0.260 | 0 | 0 | 0 | 111 | 120 | −13 |
| 85/15 | 6.6 | 5.8 | 0.142 | 0.221 | 0.4 | 4.4 | 0.075 | 107 | 110 | −9 |
| 75/25 | 6.3 | 5.1 | 0.125 | 0.195 | 0.7 | 5.1 | 0.125 | 110 | 108 | −6 |
| 70/30 | 6.2 | 4.9 | 0.117 | 0.182 | 0.8 | 5.4 | 0.150 | 137 | 124 | −6/87[a] |
| 65/35 | 6 | 4.5 | 0.108 | 0.169 | 1 | 5.8 | 0.175 | 131 | 120 | −2/113[a] |
| 60/40 | 5.3 | 4.2 | 0.100 | 0.156 | 1.7 | 6.1 | 0.200 | 115 | 126 | – |
| 50/50 | 4.3 | 3.6 | 0.083 | 0.130 | 2.7 | 7.6 | 0.250 | 134 | 132 | – |
| 40/60 | 3.3 | 2.8 | 0.067 | 0.104 | 3.7 | 8.3 | 0.3 | 139 | 132 | – |
| 25/75 | 2 | 1.7 | 0.042 | 0.065 | 5 | 9.4 | 0.375 | 116 | 126 | – |
| 0/100 | 0 | 0 | 0 | 0 | 7 | 10.3 | 0.499 | 74 | 95 | 114 |
| 75 a/25 | 6.3 | 10.2 | 0.125 | 0.195 | 0.7 | 0 | 0.125 | 137 | 131 | −3 |
| 75/25 a | 6.3 | 0 | 0.125 | 0.195 | 0.7 | 10.2 | 0.125 | 138 | 134 | −1 |
| 75 p/25 | 6.3 | 5.1 | 0 | 0.264 | 0.7 | 5.1 | 0.125 | 111 | 121 | −17 |
| 75/25 c | 6.3 | 5.1 | 0.125 | 0.195 | 0.7 | 5.1 | 0.125 | 127 | 130 | – |

[a] Two separate $T_g$'s could be observed.

nitrogen at the outer end, provides a temperature of about 0 °C at the loci of the sample.

For the *preferential staining* of the PBA phase by $RuO_4$, the samples were prepared at RT using the following procedure. The original latex with a solid content of 45% solids was diluted into a 2 wt.% aqueous solution of UAc and placed onto a Cu grid. The sample was then exposed to the $RuO_4$ vapor before completely drying. The vapor was generated by the reaction of ruthenium (III) chloride hydrate (Aldrich) and a commercial household bleach (5.25% solution of sodium hypochlorite). All samples were dried at RT for another 24 h before using them for the TEM measurements.

For the *Pt shadow-casting* the sample was prepared by diluting the original latex (45% solids) with DI water. The latex was then mixed with a small amount of standard polystyrene (PS) spheres with a narrow particle size distribution and a known particle radius $R = 98$ nm as an internal standard. A small droplet of the mixture was then placed onto a Cu grid and dried at RT. The sample was exposed in a special high vacuum ($10^{-5}$ Torr) unit to the Pt vapor.

For the *selective staining of the carboxyl groups* of latex containing acrylic acid with CsOH, a 2 wt.% aqueous solution of CsOH (Aldrich) was used. For this purpose, the samples were prepared as described above for the preferential staining using UAc.

### *2.4.2. Sample preparation for NMR experiments*

For the determination of the particle morphology via solid state $^1$H NMR spin diffusion NMR experiments, all samples were freeze-dried with liquid nitrogen under vacuum from the original latex to maintain the original particle morphology. The freeze-dried latex was packed in a 7 mm rotor and placed in an NMR spectrometer. All measurements were made at RT as well as at 60 °C.

### 2.5. NMR measurements

Spin-diffusion experiments [8, 12, 13] are typically exchange experiments with an evolution or selection phase, with a mixing time, $t_m$, during the spin-diffusion processes, and with a detection period. For short diffusion times, the mean-square distance $\langle x^2 \rangle$ that the magnetization moves within the time $t_m$ is given by $\langle x^2 \rangle = aDt_m$, where $D$ is the spin-diffusion constant of the system under study. The factor '$a$' depends on the geometry of the packing (e.g. lamellar, cylindrical, or spherical) [14]. The spin-diffusion constant is related to the strength of the dipolar coupling as reflected in the line width of the $^1$H NMR spectrum [15]. This relationship is based on calibration using polymers of different molecular mobilities by comparing spin-diffusion data with direct measurements of domain sizes by X-ray scattering and electron microscopy [14, 15]. Thus, spin diffusion is particularly suited for characterization of small domains, nanoheterogeneities, or concentration fluctuations on length scales of a few nanometers, where other methods often fail owing to limitations in resolution or contrast. Spin diffusion requires that the different components contained in the sample can be distinguished in their NMR parameters [8]. This is particularly straightforward if the components differ in mobility or in chemical shifts in the proton spectrum. For a system with different mobilities, the dipolar filter technique selects regions with mobility differences of the components. The dipolar filter is a pulse sequence consisting of 12 pulses separated by a delay time, $t_d$, varying from 2 to 80 μs. The different filter strengths allow the characterization of a gradual interphase in the particle [10]. A weak filter corresponds to a short $t_d$, and a strong filter corresponds to a long $t_d$. For short $t_d$, most of the rigid components with strong dipolar couplings are already suppressed. With increasing $t_d$ values the filter becomes stronger and compo-

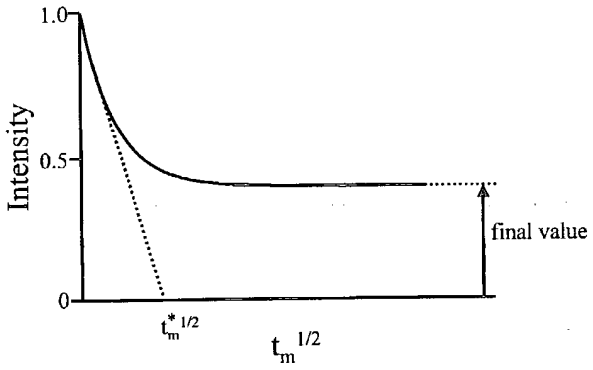


Fig. 1. Typical type of spin-diffusion curve with illustration how to determine the final value and $t_m^{*1/2}$.

nents of different mobilities can be specifically selected. Since the mobility of the soft components is reduced in the interphase, this amount is also reduced by the dipolar filter. By contrast, the mobilized portion of the rigid components immersed in the mobile phase is still detected after applying a weak filter (short $t_d$). By choosing a strong filter (long $t_d$), the rigid component including the interphase is suppressed and only very mobile regions are selectively detected. In the $^1H$ spectra the mobile component detected as a narrow line can be quantified easily. The evaluation of the rigid component from these spectra is inaccurate because of the broad lines with line widths up to about 50 kHz. The intensity of the mobile component has to be corrected by the longitudinal relaxation time $T_1$ and is then plotted versus the square root of mixing time ($t_m^{1/2}$). A typical curve is shown in Fig. 1.

For a quantitative evaluation [10, 11], two values (the final value and $t_m^{*1/2}$) can be determined from the graph and used for interpretation of the data and for calculation of the volume to interface ratio $(V_{tot}/S_{tot})\phi_A$. For a certain filter strength, the final value of the curve corresponds to the amount detected as mobile with this filter. In most of the measurements shown in this paper, the spin-diffusion curve reached an equilibrium value during the time of measurement. Otherwise it could be extrapolated easily. Taking into account the approximation given in [14] and assuming that the proton densities in phases A and B are the same, the ratio $(V_{tot}/S_{tot})\phi_A$ can be calculated [14] as:

$$\frac{V_{tot}\phi_A}{S_{tot}} = \frac{1}{\phi_B}\,\frac{2}{\sqrt{\pi}}\,\frac{\sqrt{D_A D_B}}{\sqrt{D_A}+\sqrt{D_B}}\,\sqrt{t_m^*} \qquad (1)$$

where

| | |
|---|---|
| $V_{tot}$ | total volume of the particle (in $nm^3$) |
| $S_{tot}$ | total interface area between phases A and B (in $nm^2$) |
| $\phi_A, \phi_B$ | proton fraction of phases A and B |
| $D_A, D_B$ | spin-diffusion coefficients of phases A and B |
| $t^*_m$ | mixing time during which spin diffusion takes place |

Please note that we are making a clear distinction between interfaces and interphases. Both are two connected structures, however, an interface is an area, whereas an interphase is a volume. All details of the concepts for the characterization of interphases in core-shell latex particles are extensively described in [10].

## 3. Results and discussion

### 3.1. The influence of the core/shell ratio on the particle morphology

#### *3.1.1. Characterization by transmission electron microscopy*

Different methods of imaging the latex particles were used: (i) Preferential staining of the PBA/PMMA soft phase with $RuO_4$. To prevent the latex particles from beam damage the samples were also negatively stained with UAc before exposing them to the $RuO_4$ vapor. (ii) To distinguish between soft and hard phases, the particles were shadowed with Pt-shadowing/casting.

(i) Preferential staining with $RuO_4$

The TEM of latex particles preferentially stained with $RuO_4$ are given in Fig. 2 for different samples with varying soft to hard phase ratios.

The TEM pictures for the 100/0 soft/hard particles is shown in Fig. 2a. The sample was prepared for TEM examination by first dilution in a aqueous solution of UAc (see section above) to enhance particle-form stability. The sample was then exposed to $RuO_4$ vapor for 15 min. As expected from the staining experiment with UAc, it is not possible to maintain the particle shape. No difference in contrast can be seen, indicating that the pure 100/0 soft phase particles are statistical copolymers with no PMMA domains.

In contrast to the 100/0 soft core/hard shell-particles, for the 75/25 the polymerization of pure PMMA was carried out in a second stage. Thus, a second PMMA phase is expected on the particle surface, and information about the degree of coverage is of interest. To obtain the TEM image shown in Fig. 2b, the emulsion was washed by ultrafiltration to remove the water-soluble oligomers. Otherwise, it was not possible to distinguish between an adsorbed and a chemically bound PMMA phase. As shown in Fig. 2b, the remaining (chemically bound) PMMA phase is not sufficient to cover all the soft phase material for the given phase ratio. This can be seen by the deviations from the spherical shape of the latex particles. In-between the PMMA "bumps" on the particle surface (light gray), the inner soft phase (darker gray) of the PBA/PMMA is visible. To determine the phase separation, a high magnification (120000 ×) was necessary.

A phase separation in particles with 65/35 soft core/hard shell can be determined more easily. This is demonstrated by the TEM image shown in Fig. 2c. Here the soft (s) to

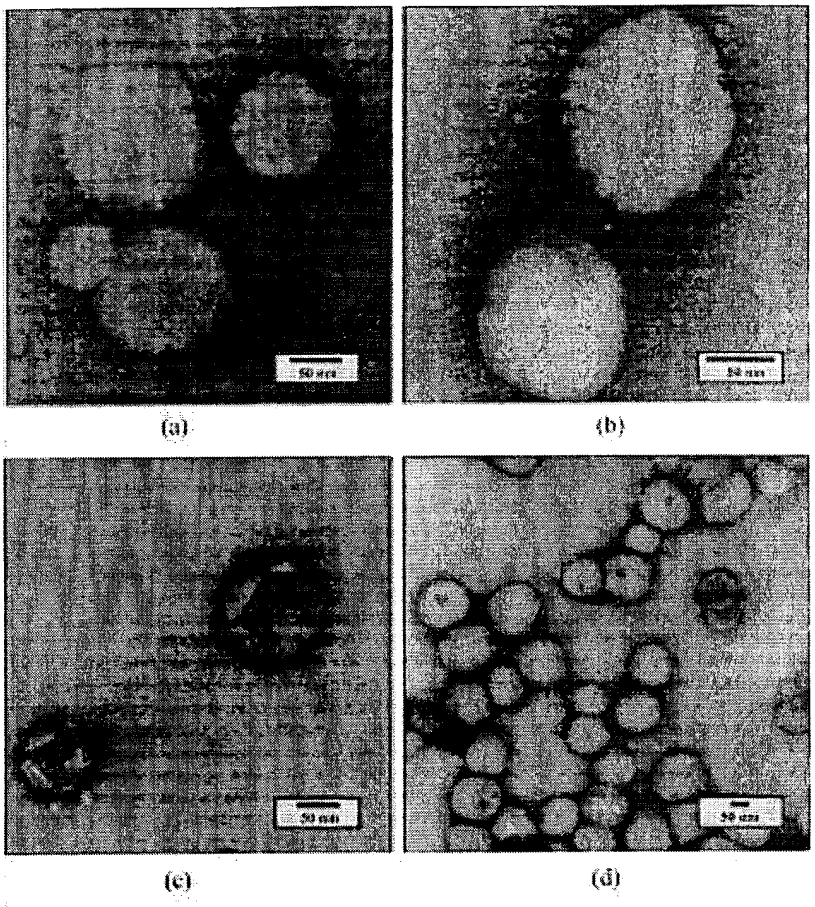


Fig. 2. TEM pictures of samples with different soft to hard phase ratio contrasted by preferential staining with $RuO_4$. All samples were additionally stained with UAc before applying the $RuO_4$ stain. Due to this staining procedure the soft, P*n*BA rich phase appears darker than a PMMA phase which is not stainable at all with $RuO_4$. Scales are given to estimate the particle size. (a) 100/0 pure soft phase particles, (b) TEM image of a cleaned sample of latex particles with a s/h phase ratio of 75/25. TEM pictures of particle with a s/h phase ratio of (c) 65/35 and (d) 50/50.

hard (h) phase ratio guarantee a particle form stability and well defined phase separated regions of PMMA and PBA/PMMA copolymer in the same particle. No water soluble polymeric components were found covering or adsorbed onto the particle surface. Thus, the preferential staining leads to differences in contrast indicated by the light gray outer PMMA region in contrast to the darker gray PBA/PMMA copolymer phase in the inner part of the particles. In contrast to the 75/25 particles, the shape is more spherical and the degree of coverage is increased.

For the latex particles with a soft to hard phase ratio of 50/50, a dramatic change in particle morphology is visible (Fig. 2 d). From the regular spherical shape and the preferential staining, one can see that now the PMMA hard phase is able to cover the soft phase of the particles almost completely. For some particles in the micrograph, the soft phase material is notable as gray spots on the particle surface. Note, this is only visible for particles laying in the right direction to the observer. From the stoechiometric ratio of the two phases, the thickness of a completely uniform shell would be expected to be 14 nm. As one can see in the picture this ideal core/shell system is not reached and this result implies, that a thick interphase between the soft PBA/PMMA and PMMA phase is most likely. In comparison to the 75/25 sample, the particles are now, like the 65/35 particles, more spherical in shape and from the lower magnification, one can see a narrow particle size distribution.

(ii) Pt-shadowing technique

The Pt-shadowing technique was applied to all samples to support the results of the preferential staining technique. This technique also allows one to judge the hardness of the individual particles. As described above, the samples were mixed with a small amount of standard polystyrene (PS)

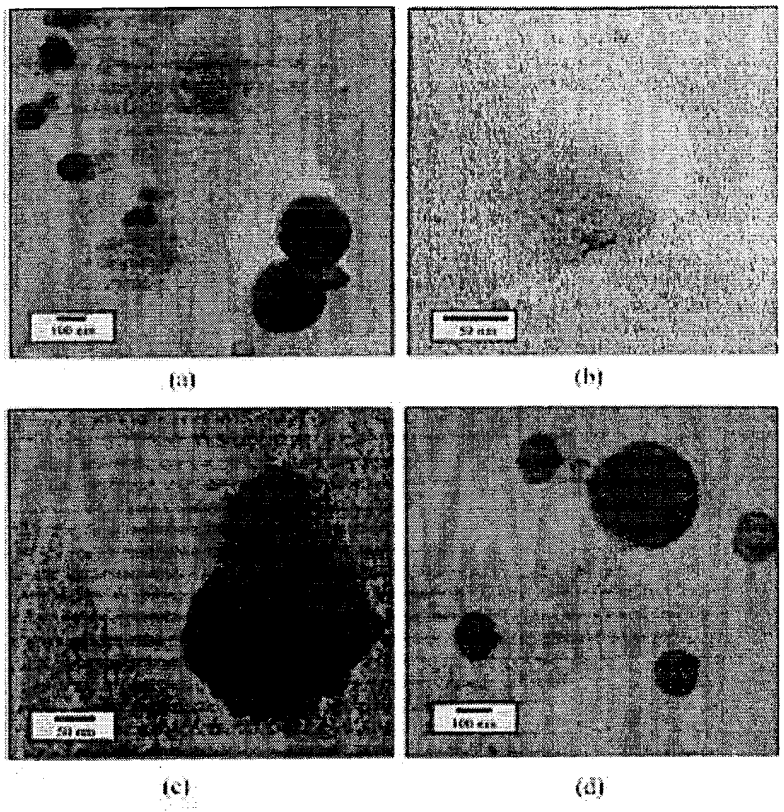

Fig. 3. TEM images of particles with different soft to hard phase ratios shadowed by Pt. The Pt-shadowing technique allows to distinguish between hard and soft phase regions. Shown are samples of (a) 100/0, (b) 75/25, (c) 65/35 and 50/50 particles. Note, in Fig. 3 a and d the PS spheres added as an internal standard can be seen. The sample shown in Fig. 3 a is a blend of 100/0 and 0/100 particles in a ratio 1 : 2.

spheres with a narrow particle size distribution and a known particle diameter of $d = 196$ nm. Under the drying conditions at RT, particles with a low $T_g$ would deform whereas high $T_g$ latex particles such as the PS standard spheres would retain their spherical shape. To monitor this behavior, a very thin layer of Pt is vaporized at a certain angle $\theta$ onto the surface of the sample. By this procedure, Pt is not deposited in the shadow of the particles which are then of a low contrast (white) in the resulting TEM picture. The length of the shadow depends on the height of the particle which is correlated to the hardness of the particle under investigation. Therefore deformed particles cast shorter shadows, beginning at the edge of each particle. Hard particles, in contrast, cast long shadows which are towing in at the particle's edge going through a maximum in width before narrowing to a tip. The maximum is directly related to the diameter of the hard particle. The particle height of soft and hard species can be calculated using the measured length of the particle's shadow and the known angle at which the sample was shadowed. The proper angle can be calculated easily from the internal PS standard particles.

In Fig. 3 the results of Pt-shadow-casting are shown for the 100/0, 75/25, 65/35 and 50/50 samples of composite latex particles. Beside the large particles in all of the TEM pictures in Fig. 3, very small particles can be found. By judging the shape of the shadow it is obvious that these particles must have a high amount of PMMA. The particle size can be calculated to be about $d \approx 10$ nm. This large amount of small particles correlates with the observation of the formation of a small component during the polymerization of the seed (data not shown). This result has been proved by NMR measurements of the particles obtained in the eluent of the washed 75/25 particles yielding a higher PMMA content in the small sized particles.

In addition to the mixture with the PS spheres, the sample in Fig. 3 a is a blend of 100/0 and 0/100 soft/hard phase ratio particles with a ratio of 1 : 2. At the right bottom of the picture two of the standard PS spheres are visible ($d = 196$ nm). The shape of the shadows is typical for those of hard spheres as discussed above. The small particles, exhibiting a shadow of the same quality as the PS spheres, are the PMMA 0/100 particles which are of a mean diameter of 74 nm (DLS). The larger, light gray particles are the PBA/

PMMA 100/0 copolymer latex particles. By contrast to the PS and PMMA spheres no shadow is detectable, indicating that the particles are completely flattened down. Estimated from the TEM pictures the particle sizes from these particles are about $d = 170$ nm. Compared to the DLS results of 153 nm the particles are flattened down due to the high content of low $T_g$ polymer (PMMA: $T_g$ = 105 °C, PBA: $T_g$ = −45 °C) which causes a process of deformation of single particles and film formation for latex system. An additional shrinkage of the particles visible in the TEM picture due to the decomposition by the electron beam has to be taken into account too. Due to this fact the differences between the estimated particle sizes from the TEM pictures and the DLS measurements are more pronounced than obvious.

In Fig. 3b, it is notable that the different phases of the 75/25 soft/hard phase ratio particle separate into two parts during the drying process. The large, light gray area at the top of the particle, having no shadow corresponds to the former soft phase of the particle. A small area with higher contrast and a short shadow correspond to the former hard phase PMMA region. In contrast to the 100/0 and 85/15 (data not shown) particles, it is proved, that phase separation occur (similar results were obtained from the preferential staining experiment).

For the 65/35 sample the phase separation is more obvious (Fig. 3c). From the length of the shadow, a particle height to diameter size ratio for the small, light gray structure with a long shadow at the top of the entire particle, can be calculated to be about 1. This correlates to the PMMA hard phase material. The broad structure of a higher contrast at the bottom of the picture has a relatively short shadow length corresponding to the soft phase material. Here, from the length of the shadow, the size ratio is calculated to be about 0.3 which confirms the ellipsoidal shape of that phase during the shadowing process. The irregular shape of the particle is a result of beam damage and does not reflect the real particle shape. The sizes can only be estimated due to the difficulty in evaluating the proper particle size because of the superposition of both shadows from the soft as well as from the hard phase region in the picture. However, it is shown here that the method of Pt shadowing is an ideal complement to the results of the preferential staining technique.

The results for the 50/50 particles (Fig. 3d, long, towing in shape of the shadows) can be discussed in the same way as the result in Fig. 3a for the pure PMMA particles. No soft phase could be seen which leads to the conclusion that for a phase ratio of 50/50 the particles are almost completely covered by the PMMA phase. The irregular shape is again a result of the beam damage.

Comparison of the TEM results

The only method to investigate directly the particle morphology by TEM measurements reported in this work is the technique of preferential staining with $RuO_4$. The major disadvantage of this method from a more general point of view is the need of different chemical reactivities of different polymeric materials with the staining agent to induce the contrast in electron density. Compared to the latter method, staining with Pt-shadowing is a indirect method, relaying on special attributes of the sample. Therefore it is possible to get indirect information on the particle morphology for phase separated latexes with a large difference in $T_g$ of the two polymer phases. The drying temperature for sample preparation should be in between these two $T_g$'s. In contrast to the preferential staining this method does not relay on the chemical reactivity, which may be of an advantage. Both methods complement one another in determining particle morphology.

As shown in the experimental part of this work, it might be necessary to separate the particles from their water-soluble oligomeric parts. These parts, referred to as a serum, may prevent the possibility to resolve a particle morphology even if the proper staining method is applied.

As a result of the different TEM staining experiments, four different kinds of morphologies can be determined:

(i) Particles with a more or less uniform distribution of the PMMA through out the particles. This is self-evident for the 100/0 particles consisting only of the soft phase copolymer. But, for the 85/15 latex particles (data not shown) no domain structures could be determined on the particle surface. Note, that the TEM might not be sensitive enough to resolve a thin PMMA layer.

(ii) Particles with a PMMA "bump" structure at the particle surface. This structure can be determined for the 75/25, as well as for the 70/30 phase ratio (data only shown for the 75/25 ratio). To obtain the information on these structures, it is necessary to clean the latex from all water-soluble compounds. An example is given by the TEM picture of the 75/25 sample.

(iii) Particles with a more spherical shape and a better distribution of the PMMA phase on the soft core surface. The soft phase is visible as broad cracks at the surface of the final particles. The particles with 65/35 and 60/40 (latter data not shown) soft to hard phase ratios belong in this category.

(iv) Particles with an almost or completely formed PMMA shell. An example is shown for the 50/50 particles (Figs. 2d, 3d) and holds for all samples with a higher content of the hard phase material.

### *3.1.2. Characterization by solid-state NMR*

The NMR spin-diffusion experiment was performed at two different temperatures, at room temperature and at 60 °C in order to get information about different structures in the latex as described elsewhere [16]. In previous papers, the spin-diffusion was carried out on particles with a homopolymer PBA core where an additional structure of the core was not detected [9, 10, 17]. In the case of a copolymer core, the internal core also has a structure which has to be characterized. This means that three different structures have to be analyzed: (1) the overall structure of the particle, (2) the interphase structure between core and shell which can be characterized with spin-diffusion experiments at 60 °C, and (3) the internal structure of the core

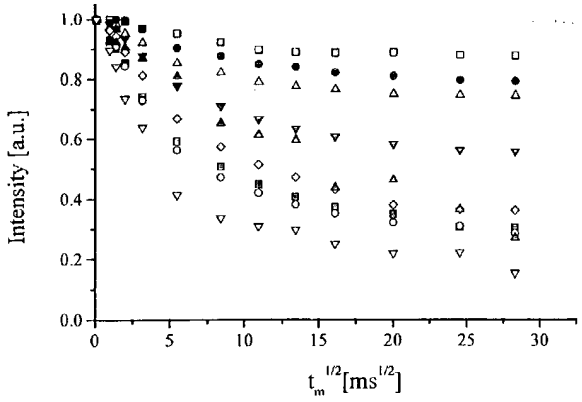


Fig. 4. Spin-diffusion curves for latex 50/50. The experiments were performed at 60 °C. The intensity of the magnetization of the mobile component is plotted versus the square root of mixing time ($t_m^{1/2}$). Nine different filter strengths were used: □2 μs; ●4 μs; △6 μs; ▼10 μs; ◇20 μs; ■30 ms; ○40 μs; ▲60 μs; ▽80 μs.

which can be better characterized with a spin-diffusion experiment at room temperature.

*Measurements at 60 °C for the detection of the core coverage and the interphase structure*

At room temperature, the spin-diffusion experiment showed a very fast decay at short mixing times and a plateau indicating that magnetization equilibrium was reached very quickly in all cases. This is due to the high spin-diffusion coefficient at that temperature. By increasing the temperature, the spin-diffusion coefficient is lowered leading to a slower spin-diffusion behavior. The temperature was chosen to be 60 °C because the one component already showed a line width in the $^1$H spectra of 400 Hz indicating high mobility and a spin-diffusion coefficient of about 0.1 nm$^2$ ms$^{-1}$. The spin-diffusion coefficient of the rigid phase was chosen to be 0.8 nm$^2$ ms$^{-1}$. The spin-diffusion curves at nine filter strength of the freeze-dried 50/50 soft core/hard shell latex are shown in Fig. 4. It has to be mentioned that at this temperature, the core itself does not show spin diffusion until a filter strength with $t_d$ = 30 μs. This means that with $t_d$ <30 μs, the magnetization of the core is not yet influenced, and the spin diffusion of the core-shell latexes takes place between the core and the shell phases. With increasing filter strength, the magnetization of the core is also influenced and the spin diffusion shows a more complicated behavior detecting two different structures. But these higher filter strengths should also give access to a detailed information of the interphase structure in the particles.

In Fig. 5, the spin-diffusion curves of the latexes with different soft core/hard shell ratios for $t_d$ = 2 μs (Fig. 5a) and $t_d$ = 80 μs (Fig. 5b) are compared. At the weak filter ($t_d$ = 2 μs), the decay at short mixing times is slow and for most of the latexes a plateau indicating a magnetization equilibrium is detected. Only the latex with the highest hard shell content (25/75) does not reach a magnetization

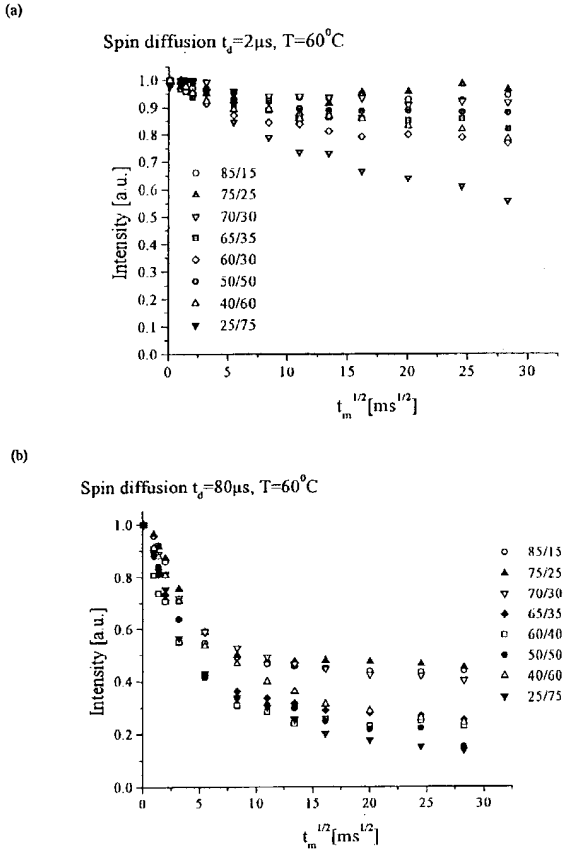


Fig. 5. Comparison of the spin-diffusion curves with a) $t_d$ = 2 μs and b) $t_d$ = 80 μs for the freeze-dried latexes with different core-shell ratios measured at 60 °C.

equilibrium indicating the existence of a large domain. In all cases, the final values of the curves are higher than the value expected from the core-shell ratio indicating that the PMMA magnetization of the shell is not entirely suppressed. The curves with the strong filter ($t_d$ = 80 μs) show two different kind of behaviors: The 85/15, 75/25 and 70/30 soft core hard shell latexes reach an equilibrium after a fast decay at short mixing time, whereas the 65/35, 60/40, 50/50 and 25/75 soft core hard shell latexes show a second decay which is slower than the first decay. This indicates the existence of a core-shell structure for the latexes with a hard shell content equal to or higher than 35%. For the latexes with a hard shell content below 35%, the shell structure is still incomplete. With increasing shell content, the final value decreases due to a smaller amount of the mobile phase in the system. The TEM results show that full coverage is obtained for latexes with a hard shell content of 50% or higher. The discrepancy between NMR and TEM may have three causes. (1) NMR measures an average. This means that if there is a mixture of particles which are covered with hard shell and particles which are nor yet fully covered, the NMR can see the two different kinds of particles. (2) Due to uncertainties in the determination of the spin-diffusion coefficients used in these experiments.

Table 2. Amount of highly mobile soft core material with a filter strength of $t_d = 80$ µs.

| Soft core/hard shell | 85/15 | 75/25 | 70/30 | 65/35 | 60/40 | 50/50 | 40/60 | 25/75 |
|---|---|---|---|---|---|---|---|---|
| Core material detected as highly mobile [%] | 52 | 60 | 57 | 39 | 38 | 44 | 57 | 52 |

Table 3. $(V_{tot}/S_{tot})\phi_A$ values calculated from the $t_m^{*1/2}$ values and the final values representing the mobile phase in the latex particles.

| Latex core/shell wt.-ratio | 2 µs [nm] | 4 µs [nm] | 6 µs [nm] | 10 µs [nm] | 20 µs [nm] | 30 µs [nm] | 40 µs [nm] | 60 µs [nm] | 80 µs [nm] |
|---|---|---|---|---|---|---|---|---|---|
| 85/15 | 300.8 | 224.6 | 147.8 | 26.6 | 15.2 | 8.5 | 7.6 | 6.3 | 5.3 |
| 75/25 | 196.2 | 76.2 | 69.5 | 29.0 | 18.4 | 16.1 | 9.9 | 7.0 | 6.0 |
| 70/30 | | 97.5 | 40.5 | 19.6 | 6.8 | 5.9 | 5.1 | | |
| 65/35 | 46.6 | 25.1 | 19.9 | 17.3 | 5.4 | 3.5 | 3.1 | 2.8 | 2.5 |
| 60/40 | 46.7 | 39.4 | 26.9 | 14.7 | 8.1 | 5.4 | 4.5 | 4.8 | 2.4 |
| 50/50 | 228.3 | 94.0 | 35.7 | 14.7 | 6.2 | 4.8 | 4.6 | | 2.8 |
| 40/60 | 49.0 | 36.8 | 14.9 | 6.9 | 4.7 | 4.3 | 3.8 | 3.4 | 3.2 |
| 25/75 | | 13.0 | 10.4 | 4.1 | 3.0 | 2.5 | 2.3 | | |

(3) For the calculation one has to assume that the interface is not very rough. It is possible that there is a high roughness due to the fact that a copolymer was used. The NMR data should be corrected by a factor to account for the interface roughness.

For a constant filter strength, the final values decreased with increasing the hard shell content. For latex 85/15, the value closest to the expected one of 0.85 is reached with a filter strength of $t_d = 6$ µs. For the other latexes, $t_d = 10$ µs is required to obtain a final value that is close to the value expected from the core/shell ratio. Only for the latex with the highest shell content, a filter strength of $t_d = 20$ µs is needed. With increasing filter strength, the final values decrease due to immobilized core material in the interphase and the core itself. The higher the shell content is, the faster is the decay of the final values. This means that with increasing shell content the phase separation is more effective and the amount of polymer with an intermediate mobilities is decreased. In Table 2, the highly mobile amount of the soft core material with a filter strength of $t_d = 80$ µs is given showing that the highly mobile amounts varies with increasing shell content. For latex 85/15, 52% of the core is mobile, while for latexes 75/25 and 70/30, a higher percentage of mobile material in the core is found. Then the value drops to about 40% for latexes 65/35, 60/40, and 50/50. As shown later, for these latexes a core-shell intact structure is detected. Compared to the latexes with a lower shell content, the interphase region between the latexes is now increased leading to a lower amount of highly mobile core material. At very high shell contents (60 and 75%), the amount of the highly mobile core material also increases indicating that a partial phase separation took place during the synthesis.

The differences of the final values of spin-diffusion curves, measured at 60 °C between $t_d = 2$ µs and $t_d = 80$ µs, are plotted in Fig. 6a which reflect the interphase region. With increasing the shell content up to 50%, the interphase

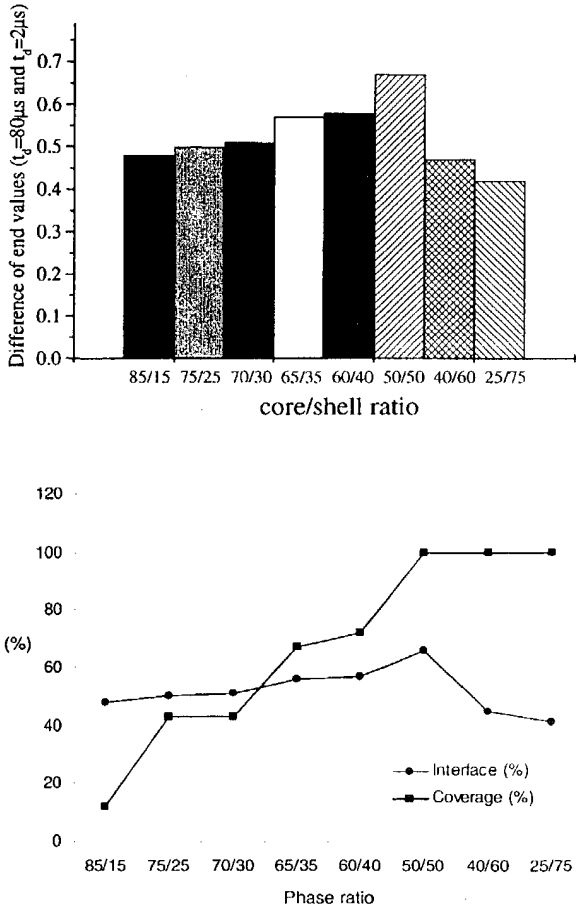


Fig. 6. a) Differences of the final values of the spin-diffusion curves measured at 60 °C with $t_d = 2$ µs and $t_d = 80$ µs reflecting the interphase region. b) Circles: % of coverage with PMMA, Squares: % of interface region, both as a function of phase ratio.

Table 4. The $(V_{tot}/S_{tot})\phi_A$ values determined from the spin-diffusion experiment and the theoretical $(V_{tot}/S_{tot})\phi_A$ values calculated from the diameter of the particles.

| Latex core/shell wt.-ratio | $(V_{tot}/S_{tot})\phi_A$ from measurement | $(V_{tot}/S_{tot})\phi_A$ theoretical for a core-shell morphology | Coverage [%] | Coverage with roughness [%] |
|---|---|---|---|---|
| 85/15 | 100.0 | 18.0 | <20 | 12 |
| 75/25 | 27.8 | 18.0 | 65 | 43 |
| 70/30 | 27.7 | 20.8 | 75 | 43 |
| 65/35 | 17.8 | 20.0 | >100 | 67 |
| 60/40 | 16.5 | 21.2 | >100 | 72 |
| 50/50 | 12.0 | 21.8 | >100 | 100 |
| 40/60 | 7.3 | 22.0 | >100 | >100 |
| 25/75 | 3.5 | 21.2 | >100 | >100 |

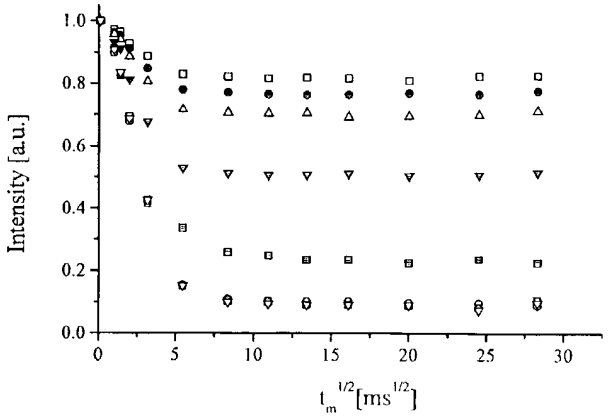


Fig. 7. Spin-diffusion curves for latex 50/50 performed at RT. The intensity of the magnetization of the mobile component is plotted versus the square root of mixing time ($t_m^{1/2}$). Nine different filter strengths were used: □2 μs; ●4 μs; △6 μs; ▼10 μs; ◇20 μs; ■ 30 ms; ○ 40 μs; ▲60 μs; ▽80 μs.

region increases as well, while at higher shell contents the interphase becomes smaller (see also Fig. 6b).

Table 3 shows the values of $(V_{tot}/S_{tot})\phi_A$ calculated after determining $t_m^{*1/2}$ from the spin-diffusion curves. The $(V_{tot}/S_{tot})\phi_A$ values drop with increasing filter strength and reach small values at $t_d = 80$ μs. Three different regions in the table can be distinguished. The gray marked region gives information about the coverage of the particles and the overall structure of the particles. The region to its left characterizes very large structures in the particles, and the region to the right gives information about the small structures in the particles, especially in the interphase.

The coverage, and so indirectly also the structure of the entire particle, can be determined if the final value is equal to the core amount. The value of $(V_{tot}/S_{tot})\phi_A$ according to the final value was determined and compared to the value obtained for the case of an ideal core-shell structure ($(V_{tot}/S_{tot})\phi_A = d_{core}/2\varepsilon$ where $\varepsilon$ is the dimension, in this case $\varepsilon = 3$). The values are shown in Table 4 along with the coverage of the core with shell material. The % coverage was first calculated by dividing values in column 3 by column 2 and multiplying the product by 100, for the case when no roughness is assumed between the core and shell. This leads to % coverage values which are too high. Thus, these values have to be corrected. For this purpose, the TEM results were used to set the 50/50 latex to have a 100% coverage. Based on this, all the other coverage values were recalculated and listed in the last column in Table 4. For latex 85/15 the coverage is low (12%), then it increases with increasing the shell content until an intact core-shell structure. An intact core-shell structure in the case of an optimal smooth interface is detected for latex 65/35, but when correction was made to account for interfacial roughness, this same latex is found to have a coverage of 67%. With increasing the shell content, the values are even lower than expected indicating a larger contact area between the two phases. It is unlikely that microdomains are already detected at this filter strength, but instead a certain roughness between the phases is possible.

From the data of the filter strengths versus $(V_{tot}/S_{tot})\phi_A$ combined with the final values given in Table 5, a profile of the particle can be obtained. The higher the $(V_{tot}/S_{tot})\phi_A$ value is, the smaller the interface area between the phases of different mobilities. For example, in the case of the 85/15 latex at a filter strength of 2 μs, 92% of the latex is detected as mobile and 8% as rigid. The interface area between the phases is very small. A large step in the $(V_{tot}/S_{tot})\phi_A$ value is detected between the filter strength of 6 and 10 μs (see Table 5). This allows for the conclusion that 12% (= the difference between the final values at 6 and 10

Table 5. The final values determined from the spin-diffusion curves at different filter strengths for the freeze-dried latexes with varying core-shell ratios measured at 60 °C. The value which is the closest to the value expected from the core-shell ratio is in bold.

| Latex | 2 μs | 4 μs | 6 μs | 10 μs | 20 μs | 30 μs | 40 μs | 60 μs | 80 μs |
|---|---|---|---|---|---|---|---|---|---|
| 85/15 | 0.92 | 0.90 | 0.87 | 0.75 | 0.64 | 0.56 | 0.54 | 0.46 | 0.44 |
| 75/25 | 0.95 | 0.89 | 0.89 | 0.76 | 0.67 | 0.65 | 0.57 | 0.51 | 0.45 |
| 70/30 | 0.91 | 0.83 | 0.78 | 0.64 | 0.48 | 0.43 | 0.40 | 0.57 | |
| 65/35 | 0.82 | 0.77 | 0.74 | 0.63 | 0.42 | 0.33 | 0.32 | 0.28 | 0.25 |
| 60/40 | 0.78 | 0.76 | 0.73 | 0.58 | 0.45 | 0.36 | 0.34 | 0.41 | 0.23 |
| 50/50 | 0.88 | 0.79 | 0.74 | 0.56 | 0.36 | 0.30 | 0.29 | 0.27 | 0.22 |
| 40/60 | 0.80 | 0.77 | 0.67 | 0.48 | 0.31 | 0.28 | 0.25 | 0.24 | 0.23 |
| 25/75 | 0.55 | 0.52 | 0.49 | 0.33 | 0.19 | 0.14 | 0.13 | | |

μs) of the particle with an intermediate mobility to create domains forming a large interphase. Whereas 13% of the particle (1 minus final value at 6 μs to get the information about the phase detected as rigid) form a bigger domain and therefore a much smaller interface between the phases.

At a high filter strength with $t_d$ = 80 μs, the spin-diffusion experiment is no longer sensitive to the entire particle structure, but only to internal morphologies. For latexes 85/15 and 75/25, the $(V_{tot}/S_{tot})\phi_A$ values given in Table 3 are 5.3 nm and 6.0 nm, respectively. For the latexes with a higher shell content, the values are between 2.4 nm and 3.2 nm. This means that for latexes 85/15 and 75/25, larger domains are detected.

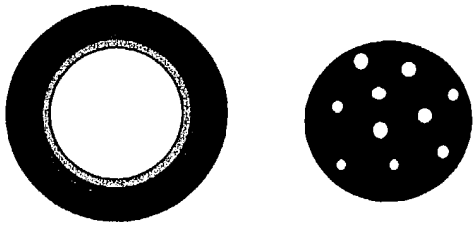

Fig. 8. a) With weak filter strengths, the spin-diffusion is sensitive to the entire structure of the particle; b) with strong filter strengths the small heterogeneities in the copolymer of the core are detected.

*Measurements at room temperature to detect the internal structure of the core*

For the selection of the soft component, in this case the PBA/PMMA copolymer core, the dipolar filter was used with one filter cycle consisting of 12 pulses separated by a delay time, $t_d$, varied from 2 μs to 80 μs. For a detailed explanation, the spin diffusion on latex 50/50 with different delay times, $t_d$, varied from 2 μs to 80 μs was chosen, and is shown in Fig. 7. The curves show a very fast single step decay at short mixing times. This is due to the fast spin diffusion at temperature (RT), but also indicates small domains. It has to be mentioned that at this temperature, the spin-diffusion coefficient is high for both phases. Depending on the filter strength represented by $t_d$, between the pulses in the filter, the spin-diffusion curves at room temperature show different behaviors. At weak filter strengths ($t_d$ = 2 μs to 6 μs), the spin-diffusion curve has a low slope at short mixing times and reaches a constant final value between 0.7 to 0.8 indicating that 70% to 80% of the particle is detected as mobile. The curves with these weak filters are sensitive to the entire structure of the particle and indicate a core-shell morphology. The spin diffusion takes place from the selected core + interphase to a thin pure shell (Fig. 8a). With an effective phase separation of both phases the final value is expected to be 0.5. This means that a portion of the PMMA of the second polymerization step is mobilized by diffusion into the preexisting copolymer core. These curves detect the whole particle with a broad interphase between the phases. Even for core-shell polymers consisting of homopolymers, diffusion of the PMMA into the PBA homopolymer phase was observed, but the diffusion is even more favorable in the case of a copolymer because of an increase in the compatibility of the phases. At a filter strength of 10 μs, the curve reaches the final value of 0.5, an expected value for the stoichiometric ratio of the components. For stronger filters (20 μs – 80 μs), the decay in the spin-diffusion curve at short mixing times is very fast and the final value drops to 0.07. With these filter strengths very small heterogeneities in the core are detected. Only 7% of the particles, probably highly PBA-rich domains in the core, are selected by the dipolar filter. Then the spin diffusion takes place to the surrounding phase in the core and the shell. The spin diffusion is no longer sensitive to the entire structure of the particles, but to the structures in the copolymer phase (Fig. 8b). These measurements show that, depending on the filter strength, it is possible for the spin-diffusion experiment to be sensitive to the entire structure of composite particles, or to be sensitive only to the structure of the mobile copolymer where one component can be the same as in the rigid phase. The greater the line width is, the more difficult it is to perform spin-diffusion experiments with stronger filters because not only the rigid PMMA, but also the PBA is suppressed. The filters strength was increased until almost no PBA was detected and it was no longer possible to perform the spin-diffusion experiment within a reasonable time. The decrease of the line width with increasing shell ratio up to 50% and the spin-diffusion curves lead to the conclusion that with increasing shell content a microphase separation is induced where PBA rich phases were formed. The final values of the other latexes show a sudden change from a high final value of $\geq$0.5 to about 0.2 in most of the cases indicating a big difference in mobility in the particles instead of a gradient in mobilities.

### 3.2. Characterization of particles with a core/shell ratio of 75/25

For the following experiments, the core/shell ratio of the latexes was kept constant, but the characteristics in the latexes were varied. Latex 75/25, which is added for comparison, represents a latex already discussed in the previous section, containing equal amounts acrylic acid in both phases (5.1 mM each stage). Latex 75/25c was synthesized with a crosslinked shell, while the latexes 75a/25 and 75/25a were prepared with 10.2 mM acrylic acid only in the core (75a/25) or only in the shell (75/25a). All these latexes consist of a soft copolymer core of 66 % PBA and 34% PMMA. One latex was prepared with a homopolymer (PBA) core (75p/25).

*3.2.1. Characterization by transmision electron microscopy*

Staining methods similar to these in 3.1.1 were used. In addition the loci of the copolymerization of the carboxylic acid groups was analyzed via staining with a 2 wt.% aqueous solution of CsOH.

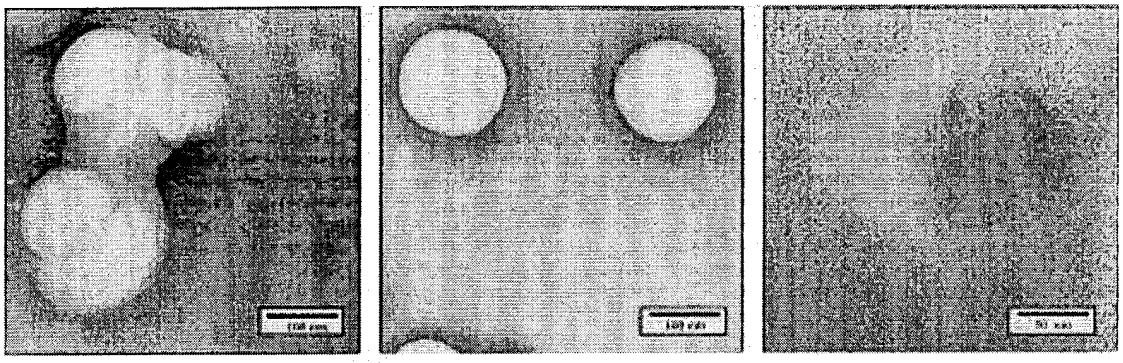

Fig. 9. TEM pictures of (a) 75p/25 and (b) 75/25c were obtained by preferential staining with $RuO_4$. For comparison we investigated sample 75/25c with Pt-shadowing, which is shown in (c).

(i) Preferential staining and Pt-shadowing technique

TEM pictures of samples 75p/25 (pure PBA soft phase) and 75/25c (crosslinked PMMA phase) are presented in Fig. 9. Differences in the final particle morphology due to the influence of thermodynamic and kinetic effects are clearly visible.

Related to the standard 75/25 recipe, the phase compatibility is decreased for the 75p/25. Due to a thermodynamic driving force, a more pronounced phase separation of the second stage polymer should occur during polymerization. The final particle morphology for the 75p/25 particles is shown in Fig. 9a. Here, as expected, a well phase separated PMMA phase could be detected.

In Fig. 9b and 9c the results for the 75/25c particles are shown using different staining methods. From Fig. 9b a spherical shape of the 75/25c particles and no staining effects by $RuO_4$ can be seen. One can assume, that an almost closed, thin PMMA shell was built up during polymerization. Fig. 9c supports this finding. Compared to Fig. 3b (75/25 standard) a longer shadow is observed in Fig. 9c, indicating a more spherical and an increased hardness of the outer parts of the particles. The final particle morphology achieved for the 75/25c particles is dominated by kinetic factors during polymerization process. The crosslinked PMMA was not able to phase separate, unlike the 75/25, due to the hindrance of polymer chain diffusion by crosslinking. Assuming a coverage of 100% of the seed, a thickness of about 10 nm for the PMMA shell can be calculated. Therefore, a decreased hardness, compared to the 50/50 particles (Fig. 3d), due to polymer diffusion of the soft phase material though thin shell is expected.

(ii) Staining with CsOH

The method of staining the carboxylic groups with CsOH gives additional information on the particle morphology. The influence of the polymer/aqueous phase interfacial tension during the polymerization can be greatly influenced by the amount and the loci of the AA copolymerized with the two main polymer phases. The staining effect of the CsOH depends on the formation of the Cs salt with the carboxylic group of the AA which increases the electron density in these regions. The formation of the Cs salt leads to three different consequences:

(i) The increase of diffusive electron scattering in these regions leads to an increased contrast (black areas) as well as an induced decomposition of the polymer material with increasing beam exposure time. This is further referred to as an etching of the particles.

(ii) From the reaction of the carboxyl groups of the AA with the Cs ions, the hydrophilicity of these areas is increased resulting in a swelling of the particles with water as a function of time.

(iii) Due to the increase of the hydrophilicity, polymer chains copolymerized with acrylic acid tend to diffuse to the outside of the particles.

In Fig. 10, the results for the 75/25 particles stained with CsOH under various preparation conditions are shown. Using a 3% aqueous solution of CsOH and mixing with a highly diluted dispersion of the 75/25 particles, leads to the result given in Fig. 10a. All particles are covered completely by a large amount of water soluble oligomers containing a high amount of acrylic acid. The picture was obtained after a 24 h of swelling and 60 s exposure time of the sample to the electron beam. It can be seen that, due to the etching effect, the oligomers are decomposed. It is not possible to determine whether acrylic acid is incorporated into the particles or not. Therefore, it was necessary to clean the sample as described before by washing with DI water.

In Fig. 10b it is shown that this cleaning procedure was successful (comparable to the procedure used for the preferential staining). In contrast to Fig. 10a, no water-soluble oligomers can be detected. Moreover, it is notable that, neither swelling of the particles (as expected if there is acrylic acid copolymerized into the particles), nor a diffusion of polymer material into the surrounding medium occur after 24 h of staining time. The result is supported by Fig. 10d which depicts the same sample area as Fig. 10b

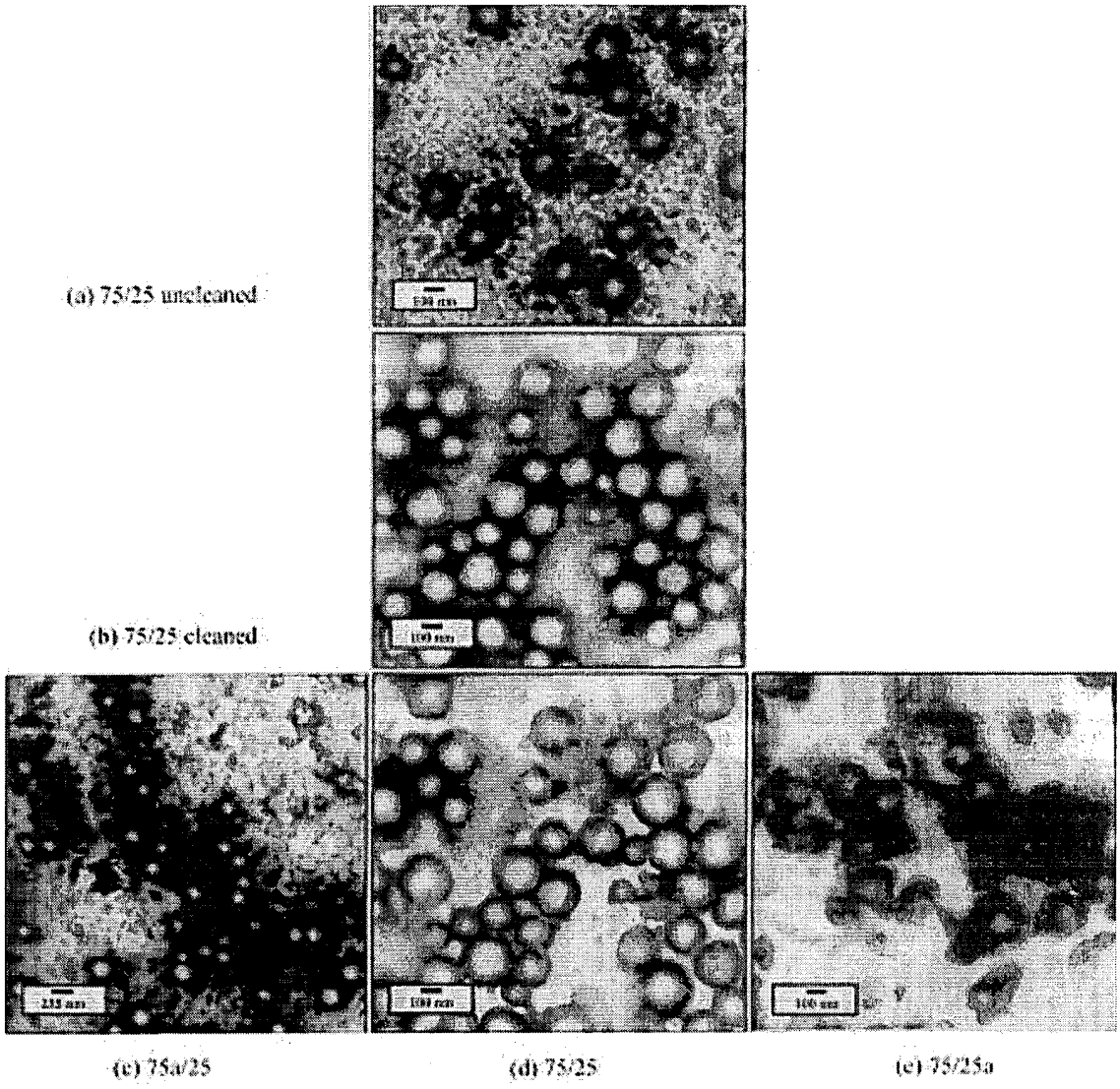


Fig. 10. TEM pictures of 75/25 particles stained by CsOH under various conditions. (a) 75/25 particles, staining time: 24 h, beam exposure time: 60 s, (b) 75/25 particles, cleaned, staining time: 24 h, beam exposure time: 0 s, (c) 75 a/25 particles, cleaned, staining time: 24 h, beam exposure time: 60 s, (d) 75/25 particles, cleaned, staining time: 24 h, beam exposure time: 60 s, (e) 75/25 a particles, cleaned, staining time: 24 h, beam exposure time: 60 s.

after a exposure time of 60 s of the latex particles to the electron beam. No significant etching effect could be observed at the particles surface. This concludes, that most of the AA which is present during the whole polymerization process stays in the water phase forming water soluble oligomeric components.

In Fig. 10c–e the results on the variation of AA is shown. All samples were cleaned as described before. TEM pictures taken for the different particles (75a/25, 75/25a) without applying the swelling procedure (data not shown), are comparable to Fig. 10b for the 75/25 particles. To obtain further information the staining time was extended to 24 h and all samples were exposed 60 s to the electron beam to induce the etching of AA rich phase regions. After this staining procedure significant differences between the three samples are visible. In Fig. 10c again polymer chains high in contrast are surrounding all particles. This is due to the increase of the hydrophilicity of polymer chains copolymerized with acrylic acid which tend to diffuse to the outside of the particles. This lead to the conclusion that for the 75a/25 particles more AA is incorporated into the polymer phase compared to the 75/25. The behavior of the 75/25a particles under the described staining procedure is different compared to the former results. As shown in Fig. 10e there are ellipsoidal shaped areas of high contrast beside the particles. A possi-

Table 6. Final values determined from the spin-diffusion curves of the latexes with a core/shell ratio of 75/25 measured at 60 °C.

| Latex | 2 μs | 4 μs | 6 μs | 10 μs | 20 μs | 30 μs | 40 μs | 60 μs | 80 μs |
|---|---|---|---|---|---|---|---|---|---|
| 75/25 | 0.95 | 0.89 | 0.89 | 0.76 | 0.67 | 0.65 | 0.57 | 0.51 | 0.45 |
| 75p/25 (RT) | 0.90 | 0.85 | 0.81 | 0.73 | 0.58 | 0.53 | 0.49 | 0.48 | 0.37 |
| 75/25c | 0.72 | 0.71 | 0.67 | 0.62 | 0.48 | 0.41 | 0.38 | 0.33 | 0.32 |
| 75a/25 | 0.80 | 0.85 | 0.76 | 0.67 | 0.52 | 0.44 | 0.44 | 0.42 | |
| 75/25a | 0.72 | 0.60 | 0.51 | 0.50 | 0.43 | 0.42 | 0.43 | 0.37 | 0.33 |

Table 7. $(V_{tot}/S_{tot})\phi_A$ values calculated from $t_m^{*1/2}$ and the final values determined from the spin-diffusion curves from the latexes.

| Latex | 2 μs [nm] | 4 μs [nm] | 6 μs [nm] | 10 μs [nm] | 20 μs [nm] | 30 μs [nm] | 40 μs [nm] | 60 μs [nm] | 80 μs [nm] |
|---|---|---|---|---|---|---|---|---|---|
| 75/25 | 196.2 | 76.2 | 69.5 | 29.0 | 18.4 | 16.1 | 9.9 | 7.0 | 5.9 |
| 75p/25 (RT) | 220.7 | 66.5 | 48.0 | 30.7 | 12.8 | 9.2 | 6.1 | 5.6 | 4.0 |
| 75/25c | 19.0 | 17.8 | 13.6 | 10.1 | 6.4 | 3.9 | 2.9 | 2.7 | 2.4 |
| 75a/25 | 23.0 | 32.0 | 18.5 | 12.4 | 5.9 | 4.6 | 4.3 | 2.1 | |
| 75/25a | 27.0 | 7.7 | 7.2 | 5.6 | 4.1 | 3.4 | 3.4 | 2.9 | 2.7 |

ble interpretation for this behavior is the assumption of a more phase separated PMMA hard phase (lower coverage of the soft phase seed) with a relatively high content of AA, which phase separate completely under the conditions of sample preparation for the TEM. Again, the amount of AA copolymerized within the polymer phase is higher than compared to the standard 75/25 particles.

### 3.2.2. *Characterization by solid-state NMR*

Measurements at 60 °C

The spin-diffusion experiments were also carried out at a higher temperature (60 °C) in order to get more detailed information about the internal morphology. Because the spin-diffusion coefficients are lower with increasing temperature, the first (fast) decay is slower and an evaluation is more accurate. For further evaluations, the experiment on latex 75 p/25 which was performed at room temperature is also included. But because of the existence of a PBA homopolymer core, the mobility of the core at room temperature is comparable with the mobility of the copolymer core at 60 °C.

In Table 6, the final values for the latexes are summarized showing that the values for each filter usually decrease in the following order: 75/25 > 75 p/25 (RT) > 75 a/25 > 75/25 c > 75/25 a. The higher final values for latexes 75/25 and 75 p/25 and even 75 a/25 at weaker filter strengths indicate that a high amount of PMMA is mobilized, whereas for latexes 75/25 a and 75/25 c, the PMMA is less affected in its mobility. Figure 11 shows the differences of the final values reflecting the interphase region (more correctly: the amount of the particle influenced in mobility). Especially in latex 75 p/25, the interfacial region is larger due to the low viscosity of the core which allows diffusion of the second stage monomer more easily.

In Table 7, the $(V_{tot}/S_{tot})\phi_A$ values calculated from $t_m^{*1/2}$ and the final values are given. From these values, the $(V_{tot}/S_{tot})\phi_A$ value for a final value of 0.75 was calculated (Table 8) showing that a core-shell structure is probably realized in latexes 75 a/25 and 75/25 c. For latex 75/25 c, a core-shell structure was also seen by TEM. Latex 75 p/25 has the lowest coverage with 53%.

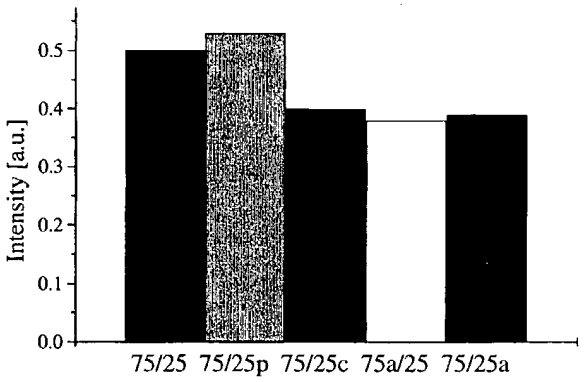


Fig. 11. Differences of the final values of the spin-diffusion curves measured at 60 °C with $t_d = 2$ μs and $t_d = 80$ μs reflecting the interphase region.

Table 8. $(V_{tot}/S_{tot})\phi_A$ values calculated for a final value 0.75.

| | 75/25 | 75p/25 | 75/25c | 75a/25 | 75/25a |
|---|---|---|---|---|---|
| $(V_{tot}/S_{tot})\phi_A$ for a final value of 0.75 [nm] | 27.8 | 34.0 | 19.0 | 17.3 | 27.0 |
| Coverage [%] | 65 | 53 | 95 | 100 | 67 |

Because very small particles were seen in the TEM pictures which could not be detected by CHDF, the latex was cleaned by serum replacement so that only the larger sized particles remained, whereas the small particles and oligomers were collected in the eluant. Both fractions were dried and then dissolved in $CDCl_3$ for solution NMR meas-

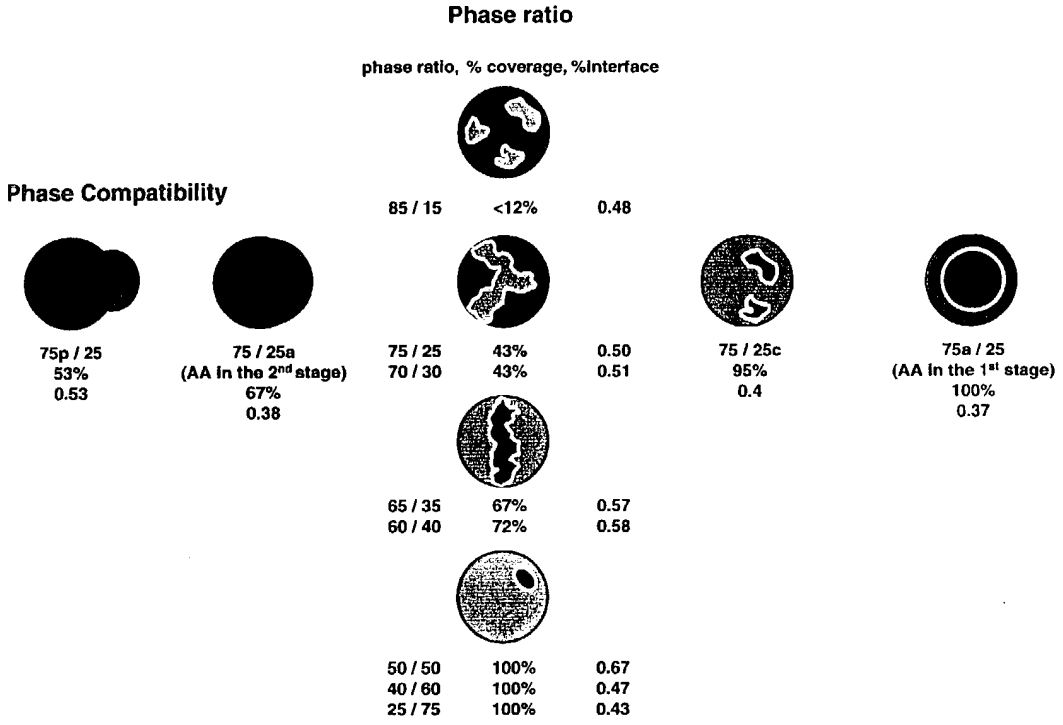


Fig. 12. Schematic representation of suggested particle morphologies based on the results from TEM and NMR for all samples under investigation. The values in the left hand side of the particles represent the interface volume obtained by NMR. The right hand side is a schematic representation of the morphology seen by TEM. The coverage by the PMMA phase obtained via NMR is given in the related description.

Table 9. Molar ratios of PBuA and PMMA in the cleaned latex and the eluant containing oligomers and very small particles. The ratio expected from the synthesis is 43.8 mole% PBuA and 56.2 mole% PMMA.

| Latex | Clean | | Eluant | |
|---|---|---|---|---|
| | PBuA [mole %] | PMMA [mole %] | PBuA [mole %] | PMMA [mole %] |
| 75a/25 | 41.2 | 58.8 | 34.7 | 65.3 |
| 75/25a | 45.0 | 55.0 | 39.9 | 60.1 |

urements. For a quantitative analysis, at least two separate peaks for each component are necessary. The peak at 3.6 ppm is clearly detected as $-OCH_3$ of PMMA, while the peak at 4.0 ppm is assigned to $-OCH_2$ of PBA.

In Table 9, the molar ratios of PBA are summarized showing that there are differences between the cleaned latex and the eluant. The ratios for the cleaned latex are very close to the expected values of 43.8 mole% PBA and 56.2 mole% PMMA. The eluant is richer in PMMA consistent with the assumption that a secondary nucleation of PMMA particles is slightly favorable. The difference between the cleaned latex and the eluant is greater in the case where acrylic acid was used in the core.

## 4. Conclusions

TEM and solid state $^1H$ spin diffusion NMR technique were used to determine particle morphology. TEM is able to resolve the particle structure with high spatial resolution even for the PBA/PMMA latex particles with only small differences in chemical reactivity for staining agents. NMR experiments support the results for the structures seen by TEM. Furthermore, NMR is a powerful tool to get detailed information on the polymer phase distribution inside the particles.

Particle morphology of PBA/PMMA composite latex particles was changed in two different ways:

(i) Increasing the phase ratio of the hard phase (PMMA) material.

(ii) Changing the morphology by varying the thermodynamic and kinetic driving forces for polymerization conditions.

The resulting particle morphologies are summarized in Fig. 12. The coverage by second stage hard phase material is increased by increasing the amount of second stage material, other reaction parameters kept constant (top to bottom). An increase of interphase region was detected as a consequence of increasing contact area. The same change in particle structure may be achieved by changing the thermodynamic (soft phase material) or the kinetic

(crosslinking) parameters. The distribution of AA between the two polymer phases may influence both parameters. The resulting particle structures are in-between the limits of 75p/25 and 75/25c. The thickness of the interphase detected by NMR reflects the polymer phase compatibility.


### Acknowledgement

Financial support from BASF AG Ludwigshafen is greatly appreciated.


### References


[1] V.L. Dimonie, E.S. Daniels, O.L. Shaffer, M.S. El-Aasser in "Emulsion Polymerization and Emulsion Polymers", P.A. Lovell and M.S. El-Aasser, editors, Wiley, Chicheston, **1997**, chapter 9, pp 293–326.

[2] Y.C. Chen, V.L. Demonie, M.S. El-Aasser, *J. Appl. Polym. Sci.* **1991**, *41*, 1049.

[3] D.C. Sundberg, A.P. Casassa, J. Pantazopoulus, M.R. Muscato, B. Kronberg, J. Berg, *J. Appl. Polym. Sci.* **1990**, *41*, 1425.

[4] Y.C. Chen, V.L. Demonie, M.S. El-Aasser, *Macromolecules* **1991**, *24*, 3779.

[5] V. Nellippan, M.S. El-Aasser, A. Klein, E.S. Daniels, J.E. Roberts, *J. Polym. Sci.: Part A: Polym. Chem.* **1996**, *34*, 3183.

[6] P. Rajatapiti, V.L. Dimonie, M.S. El-Aasser, *Polym. Mat. Sci. Eng.* **1994**, *71*, 57.

[7] H.J. Sue, E.I. Garcia-Meitin, B.L. Burton, C.C. Garrison, *J. Polym. Sci.: Part B: Polym. Physics* **1991**, *29*, 1623.

[8] K. Schmidt-Rohr, H.W. Spiess, "Multidimensional Solid-State NMR and Polymers", Academic Press, London **1994**.

[9] K. Landfester, C. Boeffel, M. Lambla, H.W. Spiess, *Macromolecules* **1996**, *29*, 5972.

[10] K. Landfester, H.W. Spiess, *Acta Polym.* **1998**, *49*, 451.

[11] F. Mellinger, M. Wilhelm, H.W. Spiess, R. Baumstark, A. Haunschild, *Macromol. Chem. Phys.* **1999**, *200*, 719.

[12] R.R. Ernst, G. Bodenhausen, A. Wokaun, *Principles of Nuclear Magnetic Resonance in One and Two Dimensions*, Oxford University Press, Oxford **1987**.

[13] D.L. VanderHart, *Makromol. Chem., Macromol. Symp.* **1990**, *34*, 124.

[14] J. Clauss, K. Schmidt-Rohr, H.W. Spiess, *Acta Polym.* **1993**, *44*, 1.

[15] S. Spiegel, K. Schmidt-Rohr, H.W. Spiess, *Polymer* **1993**, *34*, 4566.

[16] K. Landfester, H.W. Spiess, *Macromol. Rapid Commun.* **1996**, *17*, 875.

[17] K. Landfester, C. Boeffel, M. Lambla, H.W. Spiess, *Macromol. Symp.* **1995**, *92*, 109.



*Received February 3, 1999*

*Final version August 11, 1999*

literature often appears to refer only to a singular $T_c$ value—"the ceiling temperature." It is clear from the discussion above that each monomer concentration has its own $T_c$ value. The apparent designation of a singular $T_c$ value usually refers to the $T_c$ for the pure monomer or in some cases to that for the monomer at unit molarity.

For many of the alkene monomers, the equilibrium position for the propagation-depropagation equilibrium is far to the right under the usual reaction temperatures employed, i.e., there is essentially complete conversion of monomer to polymer for all practical purposes. Table 3-13 shows the monomer concentrations at 25°C for a few monomers [65–68]. Data are also shown for the ceiling temperatures of the pure monomers. The data do indicate that the polymer obtained in any polymerization will contain some concentration of residual monomer as determined by Eq. 3-173. Further, there are some monomers for which the equilibrium is not particularly favorable for polymerization, for example, α-methylstyrene. Thus, at 25°C a 2.2 molar solution of α-methylstyrene will not undergo polymerization. Pure α-methylstyrene will not polymerize at 61°C. Methyl methacrylate is a borderline case in that the pure monomer can be polymerized below 220°C but the conversion will be appreciably less than complete. Thus, for example, the value of $[M]_c$ at 110°C is 0.139 molar [41]. Equations 3-173a and 3-173b apply equally well to ionic chain and ring-opening polymerizations as will be seen in subsequent chapters. The lower temperatures of ionic polymerizations offer a useful route to the polymerization of many monomers which cannot be polymerized by radical initiation because of their low ceiling temperatures. The successful polymerization of a previously unpolymerizable monomer is often simply a matter of

**Table 3-13 Polymerization-Depolymerization Equilibria**[a]

| Monomer | $[M]_c$ at 25°C | $T_c$ for pure monomer (°C) |
|---|---|---|
| Vinyl acetate | $1 \times 10^{-9}$ | – |
| Methyl acrylate | $1 \times 10^{-9}$ | – |
| Styrene | $1 \times 10^{-6}$ | 310 |
| Methyl methacrylate | $1 \times 10^{-3}$ | 220 |
| α-Methylstyrene | 2.2 | 61 |

[a]Data are from [65-68].